O 2pπ, Si 3p, and C 2p Interaction in the Highest Energy Occupied Molecular Orbitals of Methylated Siloxanes

J. A. Tossell,*,† J. H. Moore,† K. McMillan,‡ and M. A. Coplan‡

Contribution from the Department of Chemistry and Biochemistry and the Institute for Physical Sciences and Technology, University of Maryland, College Park, Maryland 20742.
Received July 9, 1990

Abstract: Momentum distributions, $\rho(q)$, for electrons in the predominantly O 2pπ HOMO's of hexamethyldisiloxane, $Si_2O(CH_3)_6$, and the methylated cyclosiloxanes $[SiO(CH_3)_2]_n$, $n = 3$ and 4, have been measured by (e,2e) spectroscopy and calculated at the RHF/3-21G* level. In contrast to the simple one-peak $\rho(q)$ observed for the $1b_1$ O 2pπ HOMO of H_2O, the HOMO's of the methylated siloxanes show experimental $\rho(q)$ with multiple maxima, a result of significant Si and C contributions. Variations in $\rho(q)$ for the various HOMO's have been analyzed by taking the Fourier transform of $\rho(q)$ to obtain position space autocorrelation functions, $B(r)$, and by plotting orbital position distributions, $\psi(r)$. For each siloxane the HOMO contains a small contribution from a p orbital on Si and a large contribution from a p orbital on C. Both the p orbital lobes on Si and those on C generate features discernible in the autocorrelation differences, $\Delta B(r)$, between the siloxanes and H_2O. The $\rho(q)$ and $\Delta B(r)$ distributions calculated for the methylated species agree reasonably well with the experimental data. Substitution of H for CH_3 in the calculations causes a significant change in both $\rho(q)$ and $\Delta B(r)$. There are only small differences between the $\rho(q)$ distributions for $Si_2O(CH_3)_6$, $Si_3O_3(CH_3)_6$, and $Si_4O_4(CH_3)_8$, but they all differ substantially from that calculated for SiH_3OH. Thus, (e,2e) spectroscopy is potentially a probe for the coordination of the O atom in siloxane molecules or on the surfaces of solid silicates.

Introduction

In (e,2e) spectroscopy or electron momentum spectroscopy cross sections for the direct knockout of a particular orbital electron by electron impact are measured and information about the orbital momentum density of the ejected electron is directly obtained. Within the plane wave impulse approximation and the frozen orbital approximation, the measured (e,2e) cross section is directly proportional to the momentum density of the ejected electron in its initial state. In the last several years much effort has been directed at investigating the degree to which the results of (e,2e) spectroscopy are in agreement with quantum mechanical calculations. In this paper, we seek to go beyond the comparison of experiment and calculations and show how (e,2e) data can be related to the structural and chemical properties of large molecules. We have previously used this technique to explore the effect of methyl and halide substitution upon the π orbitals of C–C double and triple bonds[1,2] and changes in the N lone pair orbitals which occurred in forming the $(CH_3)_3N{-}BF_3$ complex.[3]

Accurate calculation of momentum distributions for the outermost orbitals of a molecule generally requires large basis sets and some means such as CI to account for correlation and relaxation in both target molecule and residual ion, as has been recently demonstrated for H_2O and NH_3.[4,5] By contrast, our interest has been focused on the changes in orbital momentum distributions arising from substitution. These seem to be well described by wave functions at the double-ζ SCF level. In addition to the directly measured momentum distributions $\rho(q)$, wave function autocorrelation functions,[6] $B(r)$, have been computed by taking the Fourier transform of $\rho(q)$. We have also examined autocorrelation differences, $\Delta B_{ij}(r) = B_i(r) - B_j(r)$, between molecular orbitals i and j. These can be analyzed[7] in terms of the orbital wave function averages $\bar{\psi}(r)$ and differences $\Delta\psi(r)$, where $\bar{\psi}(r) = [\psi_i(r) + \psi_j(r)]/2$ and $\Delta\psi(r) = \psi_i(r) - \psi_j(r)$. In the case of ethyne and 2-butyne, $\Delta B(r)$ plots obtained from the experimental momentum distributions could be interpreted in terms of delocalization of the π orbital of 2-butyne onto the exterior carbon atoms.[1] A similar analysis was carried out for the vinyl halides.[2]

The gaseous open chain siloxanes and cyclosiloxanes are interesting from a number of points of view. It is well established that an O atom bridging between two Si atoms is less basic than is O in H_2O.[8] The reduction in basicity of O in Si compounds has often been interpreted in terms of Si–O d–pπ bonding[9] although this theory has now been substantially modified by its developer[10] and has been criticized by numerous theoreticians.[11] In the same way that previous (e,2e) studies on NH_3 and CH_3NH_2 were able to elucidate $-CH_3$ character in the predominantly N 2p HOMO,[12] we expect to identify the nature of Si (and C or H) participation in the siloxane HOMO using experimental $\rho(q)$ and theoretical calculations of both $\rho(q)$ and orbital amplitudes.

Changes in properties from one siloxane to another, particularly for the cyclic oligomers with 2, 3, and 4 Si atoms in the ring, are also of considerable interest. Although the ring structures in most crystalline silicates contain larger numbers of Si atoms, typically 6 or 8, smaller oligomers of the type $(SiOR_2)_n$, $n = 3$ and 4, have been identified in the IR/Raman spectra of amorphous SiO_2[13] and molecular dynamics simulations indicate substantial concentrations of such small ring species in the bulk, with their concentrations increasing further approaching the surface.[14] The reactivity of the Si–O–Si linkage toward hydrolysis is much greater for the "3-ring" ($n = 3$) than for the "4-ring", and the presence of such reactive species, perhaps even the "2-ring" $Si_2O_2R_4$, may greatly affect the strength of silicate glasses.[15] Although the

† Department of Chemistry and Biochemistry.
‡ Institute for Physical Sciences and Technology.

(1) Goruganthu, R. R.; Coplan, M. A.; Leung, K. T.; Tossell, J. A.; Moore, J. H. *J. Chem. Phys.* **1989**, *91*, 1994.
(2) Goruganthu, R. R.; Coplan, M. A.; Moore, J. H.; Tossell, J. A. *J. Chem. Phys.* **1988**, *89*, 25.
(3) McMillan, K.; Coplan, M. A.; Moore, J. H.; Tossell, J. A. *J. Phys. Chem.* **1990**, in press.
(4) Bagawan, A. O.; Brion, C. E.; Davidson, E. R.; Feller, D. *Chem. Phys.* **1987**, *113*, 19.
(5) Bagawan, A. O.; Mueller-Fiedler, R.; Brion, C. E.; Davidson, E. R.; Boyle, C. *Chem. Phys.* **1988**, *120*, 335.
(6) Weyrich, W.; Pattison, P.; Williams, B. G. *Chem. Phys.* **1979**, *41*, 217.
(7) Tossell, J. A.; Moore, J. H.; Coplan, M. A. *J. Electron Spectrosc.* **1981**, *22*, 61.
(8) West, R.; Whatley, L. S.; Lake, K. J. *J. Am. Chem. Soc.* **1961**, *83*, 761.
(9) Cruickshank, D. W. J. *J. Chem. Soc.* **1961**, 5486.
(10) Cruickshank, D. W. J. *J. Mol. Struct.* **1985**, *130*, 177.
(11) (a) Bartell, L. S.; Su, L. S.; Yow, H. *Inorg. Chem.* **1970**, *9*, 1903. (b) Kutzelnigg, W. *Angew. Chem., Int. Ed. Engl.* **1984**, *23*, 272. (c) Bock, H. *Angew. Chem., Int. Ed. Engl.* **1989**, *28*, 1627.
(12) Tossell, J. A.; Lederman, S. M.; Moore, J. H.; Coplan, M. A.; Chornay, D. J. *J. Am. Chem. Soc.* **1984**, *106*, 976.
(13) Galeener, F. L. *Solid State Commun.* **1982**, *44*, 1037.
(14) (a) Garofalini, S. H. *J. Non-Cryst. Solids* **1984**, *63*, 337. (b) Garofalini, S. H. *J. Non-Cryst. Solids* **1990**, in press.
(15) Michalske, T. A.; Bunker, B. C. *J. Appl. Phys.* **1984**, *56*, 2686.

0002-7863/91/1513-1031$02.50/0

Table I. Equilibrium Geometries Calculated at the 3-21G** RHF Level Compared with Experimental X-ray Diffraction and Electron Diffraction Geometries

	R(Si-O), Å	∠Si-O-Si, deg
$Si_2O_2H_4$ calcd (D_{2h})	1.655	91.3
$Si_2O_2Mes_4$ XRD[a]	1.66	86
$(SiOH_2)_3$ calcd (D_{3h})	1.630	133.4
$(Si(Me)_2O)_3$ ED[b]	1.635	131.6
$(SiOH_2)_4$ calcd (D_{4h})	1.614	159.8
$(SiOH_2)_4$ calcd (S_4)	1.619	149.8
$(SiOH_2)_4$ ED (S_4)[c]	1.628	148.6
$(SiO(Me)_2)_4$ ED (S_4)[b]	1.622	144.8

[a] Reference 29. [b] Reference 19. [c] Reference 30.

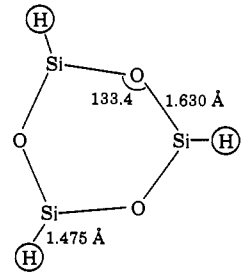

Figure 1. Calculated RHF 3-21G** equilibrium geometry of $(SiOH_2)_3$.

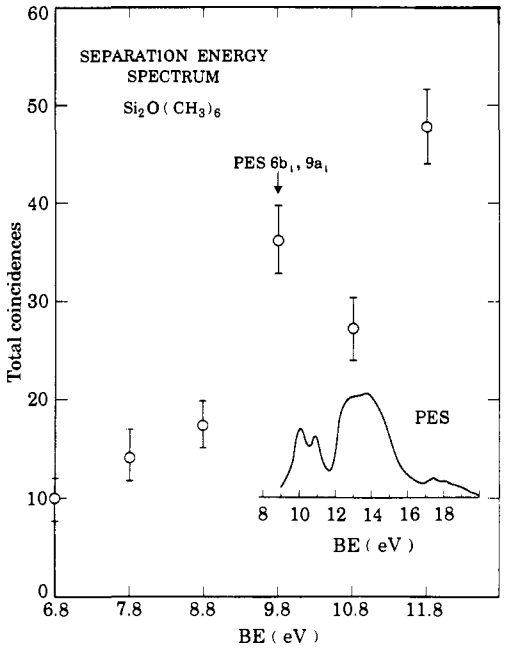

Figure 2. Separation energy spectrum for $Si_2O(CH_3)_6$ with PES (ref 25) as an inset. The total number of coincidences summed over all 25 momentum values sampled by the (e,2e) spectrometer is plotted as a function of binding energy.

presence of such ring species can be monitored by IR/Raman and by NMR spectroscopy[16] and their structure and stability calculated with using MO methods[17] or molecular dynamics simulations, directly monitoring the electron distributions in their HOMO's could be of substantial value both in their identification and in explaining their reactivity, keeping in mind that their overall basicity may well be influenced by other orbitals besides the HOMO.

We have previously reported optimized geometries, NMR properties, and some vibrational properties for the $(SiOH_2)_n$ (n = 2-4) species.[18] In Table I we compare our geometries calculated at the RHF/3-21G** level with experiment. The calculated geometry of $(SiOH_2)_3$ is shown in Figure 1. For $Si_4O_4H_8$ we have calculated optimized geometries for both D_{4h} symmetry and the S_4 symmetry which seems to best describe the electron diffraction data.[19] Although our calculated energies for D_{4h} and

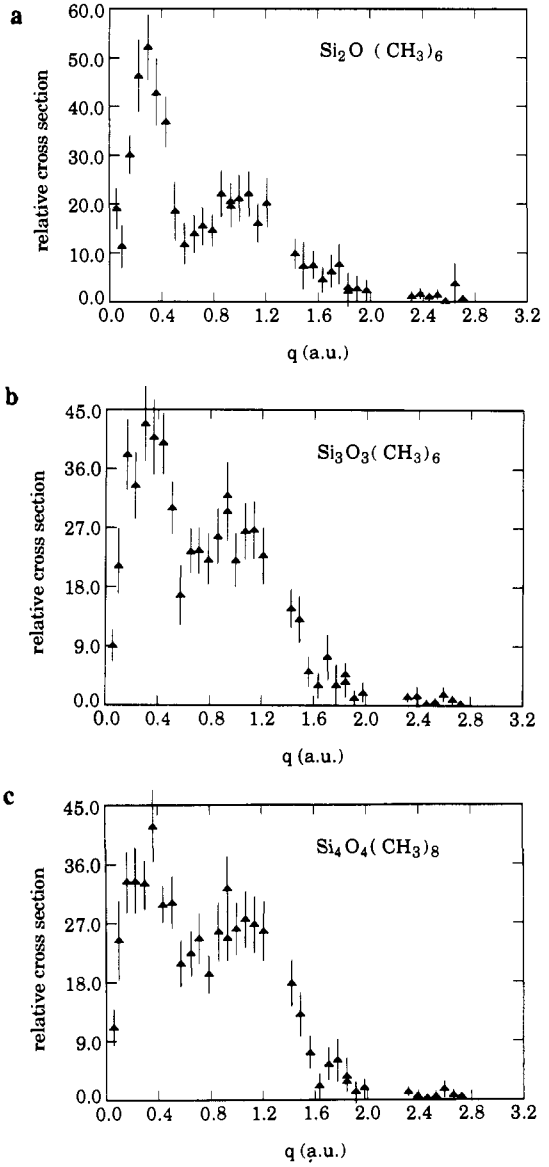

Figure 3. (a) Experimental $\rho(q)$ at 9.3 eV for $Si_2O(CH_3)_6$. (b) Experimental $\rho(q)$ at 10.0 eV for $Si_3O_3(CH_3)_6$. (c) Experimental $\rho(q)$ at 10.5 eV for $Si_4O_4(CH_3)_8$. The error bars represent one standard deviation in the relative cross section.

Table II. Calculated and Experimental Binding Energies (eV) for the HOMO in H_2O and Various Siloxanes

	$-\epsilon_i$	exp BE[a]	calcd ∠Si-O-Si
H_2O	13.28	12.61	
Si_2OH_6	12.07	11.19	144
$(SiOH_2)_2$	11.99		91
$(SiOH_2)_3$	11.74		133
$(SiOH_2)_4$, D_{4h}	11.62		160
$(SiOH_2)_4$, S_4	11.79		150
$Si_2O(CH_3)_6$	10.60	9.80	assumed 180
$Si_3O_3(CH_3)_6$	10.45	9.70	assumed 133
$Si_4O_4(CH_3)_8$, D_{4h}	10.44	9.70	assumed 160

[a] Reference 25.

(16) Brinker, C. J.; Kirkpatrick, R. J.; Tallant, D. R.; Bunker, B. C.; Montez, B. *J. Non-Cryst. Solids* **1988**, *99*, 418.
(17) (a) O'Keeffe, M.; Gibbs, G. V. *J. Chem. Phys.* **1984**, *81*, 876. (b) Kudo, T.; Nagase, S. *J. Am. Chem. Soc.* **1985**, *107*, 2589.
(18) Tossell, J. A. *J. Non-Cryst. Solids* **1990**, *120*, 13.

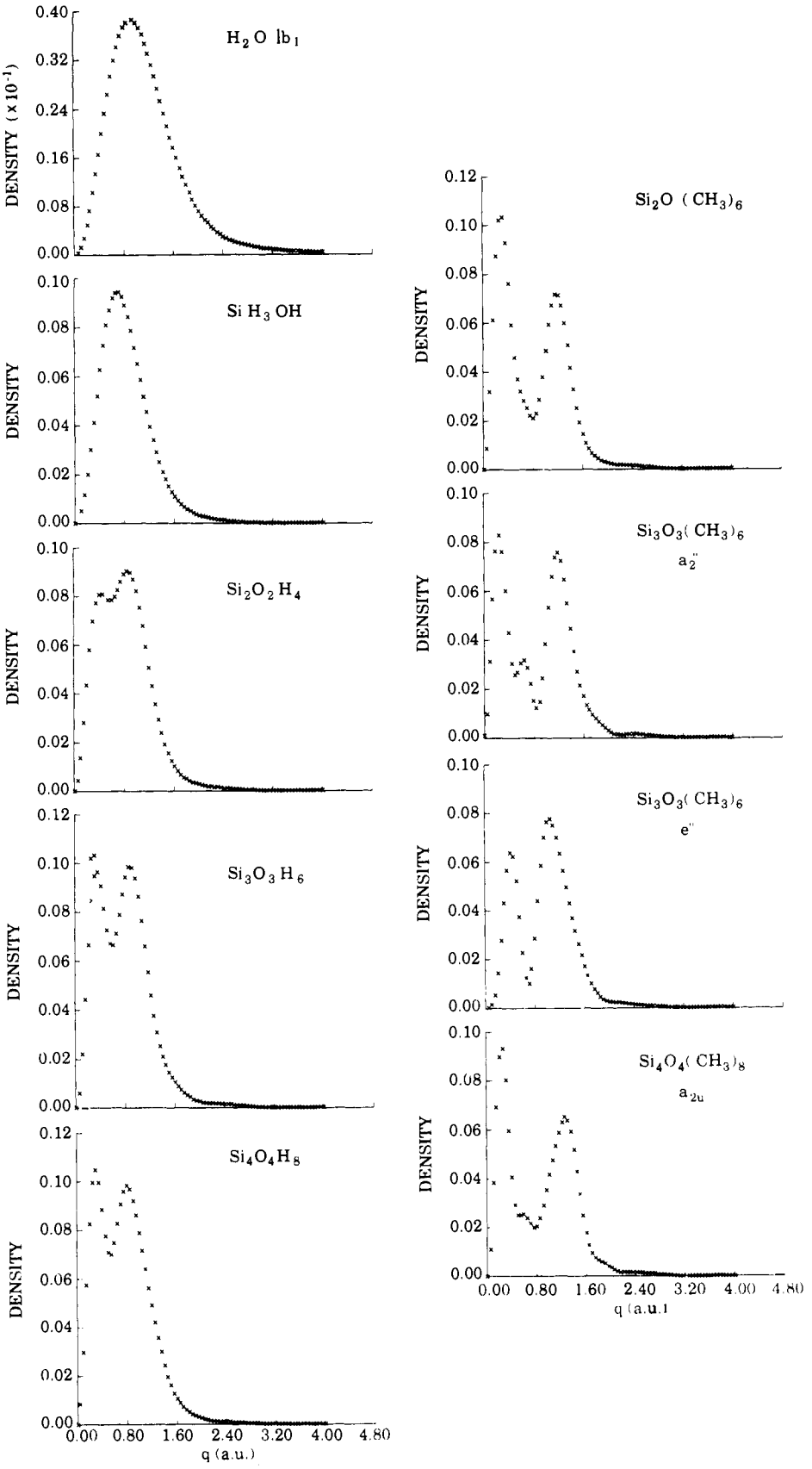

Figure 4. Calculated momentum density $\rho(q)$ for highest energy occupied molecular orbitals of H_2O and siloxanes (using 3-21G** bases and geometries described in the text).

S_4 symmetry are within 1 kcal/mol of each other the Si–O bond distances and Si–O–Si angles are substantially different. We have also carried out calculations with diffuse s,p functions[20] added to the O atoms for $(SiOH_2)_3$ at the 3-21G** optimized geometry and have calculated a 3-21G** RHF wave function for SiH_3OH at its optimized geometry. Finally, to make a more direct comparison with our experimental data we have replaced H by CH_3 for a linear Si–O–Si geometry of disiloxane $Si_2O(CH_3)_6$ and for

both the "3-ring" and "4-ring" species $(SiO(CH_3)_2)_n$, $n = 3$ and 4, using 3-21G** optimized Si,O ring geometries, experimental $Si-CH_3$ geometries, a 3-21G* basis on Si and O, and 3-21G bases on the CH_3 group (except for the "4-ring" case in which we had to revert to a STO-3G basis on the H atoms). All SCF-MO calculations were performed with the program GAMESS[21] and spherically averaged momentum densities were calculated with use of the algorithms of Epstein[22] and Kaijser and Smith.[23] Autocorrelation functions, $B(r)$, were obtained by numerical Fourier transformation of calculated momentum distributions[7] over the range 0–4 au of momentum.

Experimental Details

The (e,2e) spectrometer has been previously described.[1-3] The siloxane samples (obtained from Aldrich) were purified by repeated freeze–pump–thaw cycles prior to use.

In general, the photoelectron spectra (PES) of the siloxanes are broad and complex[24,25] but the HOMO is in all cases assigned to an orbital of predominant O $2p\pi$ character. In Table II we give calculated values of $-\epsilon_i$ for the HOMO's of H_2O and various siloxanes, along with the experimental binding energy (BE) values. Multiplying $-\epsilon_i$ by the standard value of 0.92 gives BE's in good agreement with experiment. For $(SiOH_2)_3$ we have also calculated the ionization energy by taking the difference between neutral and cation energies (with the cation studied at the UHF level), obtaining a value of 11.34 eV, 0.4 eV lower than the Koopmans' theorem estimate. For all the cyclic siloxanes, $(SiOR_2)_n$, whether methylated or not, the n highest occupied MO's are always of π symmetry with respect to the ring and of predominant O 2p character. The energy splitting within this set of n HOMO's is on the order of an electronvolt or less, e.g. 0.7 eV calculated in $[SiO(CH_3)_2]_3$. The next deeper orbital is typically separated from this set of n O $2p\pi$ orbitals by more than 1 eV. Given our finite energy resolution we cannot completely separate contributions from the n HOMO's of the cyclic compounds, but by sitting on the low-energy side of the first peak in the separation energy spectrum we can substantially increase the relative contribution of the actual HOMO to our experimental $\rho(q)$.

For $Si_2O(CH_3)_6$, for which we have calculations only in D_{3h} symmetry, the two highest MO's are a degenerate O $2p\pi$ set. Although the Si–O–Si unit in $Si_2O(CH_3)_6$ probably has a nonlinear ∠Si–O–Si, at least on a short time scale, its barrier to linearity is quite small and at least some of the properties of $Si_2O(CH_3)_6$ can be interpreted with a linear Si–O–Si model.

Results

In Figure 2 we show the separation energy spectrum of $Si_2O(CH_3)_6$ along with the experimental PES as an inset. The binding energy scale is calibrated against the 15.8 eV argon 3p peak. The maximum in the separation energy spectrum at a BE of 9.8 eV is in good agreement with the reported position of the first band of the photoelectron spectrum. The band at 9.8 eV of the PES was assigned to two MO's, $6b_1$ and $9a_1$ for a C_{2v} geometry $Si_2O(CH_3)_6$ molecule. Data were collected at a binding energy of 9.3 eV to reduce overlap with the second band of the PES, at 10.65 eV, and are shown in Figure 3a. Assuming that our experimental energy resolution can be described by a Gaussian function with a full width at half maximum of 1.4 eV, the contribution to $\rho(q)$ at 9.3 eV from the 10.65-eV band would be only 11% as large as that from the 9.8-eV band. Since the orbitals with binding energy 10.65 eV are calculated to have roughly the same shape $\rho(q)$ as the HOMO (two peaks below 1.0 au with fairly equal intensity) their perturbation of the 9.3-eV BE data should be quite small. The experimental $\rho(q)$ in Figure 3a shows a two-peak distribution with a major maximum at a momentum of about 0.3 au and a broad secondary maximum at about 1.0 au of momentum

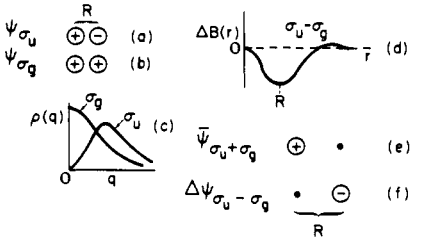

Figure 5. Pictograms illustrating the relationship of $\psi(r)$, $\rho(q)$, $\Delta B(r)$, $\bar{\psi}(r)$, and $\Delta\psi(r)$ for the σ_g and σ_u orbitals obtained by linear combination of s valence orbitals in a homonuclear diatomic.

(1 au of momentum is the momentum of the H atom ground state). The same structure is seen in the calculated $\rho(q)$ for $Si_2O(CH_3)_6$ in Figure 4, although the high-momentum peak is higher and narrower in the calculation.

In Figure 3, parts b and c, we show momentum distributions obtained at binding energies of 10.0 and 10.5 eV for $[SiO(CH_3)_2]_n$, $n = 3$ and 4, respectively. For the cyclotrisiloxane we thus sample the three highest energy occupied orbitals, of a_2'' and e'' symmetry, whose calculated momentum distributions are also shown in Figure 4. By acquiring data at the low-energy edge we weight the a_2'' distribution more heavily. Both the a_2'' HOMO and the e'' MO for $Si_3O_3(CH_3)_6$ show a two-peak structure with a suggestion of a third, intermediate peak for the a_2''. The experimental $\rho(q)$ in Figure 3b indeed shows a two-peak structure with the low momentum peak about a third larger in intensity. There is also a suggestion of a weaker intermediate peak or shoulder. The experimental and calculated momentum distributions are thus in semiquantitative agreement for $Si_3O_3(CH_3)_6$, the main difference being that the high-momentum peak is broader and lower in the experimental data. In the same way the experimental $\rho(q)$ at a binding energy of 10 eV for $Si_4O_4(CH_3)_8$ matches the calculated a_{2u} HOMO $\rho(q)$ reasonably well for the D_{4h} symmetry model (unfortunately lower symmetry structures for $Si_4O_4(CH_3)_8$ were beyond our computational capabilities). Although both the experimental and calculated $\rho(q)$ are similar in hexamethyldisiloxane and the permethylated cyclosiloxanes, the relative intensities of the high-momentum peaks are larger in the cyclic compounds.

A comparison of calculated $\rho(q)$ for the highest occupied orbitals of the siloxanes and related molecules shows a number of interesting features, which can be seen in Figure 4. For both the HOMO of H_2O and that of SiH_3OH we see only a single peak in $\rho(q)$ while for all the siloxanes in which O is coordinated by two Si's we see at least a shoulder (in Si_2OH_6) and generally a two- or three-peak structure. All molecules in the series $(SiOH_2)_n$, $n = 2$–4, show the same two-peak structure with the relative intensity of the low-momentum peak increasing as n increases. Similarly, in the calculations the low-momentum peak increases in relative intensity from $Si_3O_3(CH_3)_6$ to $Si_4O_4(CH_3)_8$. By contrast the experimental data for the methylated cyclosiloxanes in Figure 3 show the relative magnitude of the low-momentum peak decreasing slightly with increasing n. It is not clear whether this is a real discrepancy, associated with the simplified D_{4h} geometry assumed for the "4-ring" for example, or whether it simply reflects a different sampling of the n orbitals close to the HOMO in the different ring compounds. We find that the addition of diffuse s and p functions to the O in $(SiH_2O)_3$ has only a slight effect on $\rho(q)$, producing a plot indistinguishable by eye from the one shown in Figure 4. For the methylated compounds the $\rho(q)$ distributions are fairly similar to those for their H analogues but the low- and high-momentum peaks have a slightly larger separation and there is now a weak peak between them. Finally, calculations at the 3-21G level are known to underestimate the low-momentum contributions to $\rho(q)$ for the $1b_1$ MO of H_2O. Addition of diffuse functions on the O reduces the discrepancy somewhat but it is only eliminated by incorporating substantial CI. Thus, overestimation of the position of the maximum for the higher q peak (at ~0.9 au in Figure 3b) is not unexpected for our moderate basis RHF calculations.

The increase in complexity of $\rho(q)$ as $Si(CH_3)_3$ groups are

(19) Oberhammer, H.; Zeil, W.; Fogarasi, G. *J. Mol. Struct.* **1973**, *18*, 309.
(20) Clark, T.; Chaudrasekhar, J.; Spitznagel, G. W.; Schleyer, P. V. R. *J. Comput. Chem.* **1983**, *4*, 294.
(21) Schmidt, M. W.; Boatz, J. A.; Baldridge, K. K.; Koseki, S.; Gordon, M. S.; Elbert, S. T.; Lam, B. *QCPE Bull.* **1987**, *7*, 115.
(22) Epstein, I. R. *Chem. Phys. Lett.* **1971**, *9*, 9.
(23) Kaijser, P.; Smith, V. H., Jr. *Adv. Quantum Chem.* **1977**, *10*, 37.
(24) Ermakov, A. I.; Kirichenko, E. A.; Pimkin, N. I.; Chizhov, Y. V.; Kleimenov, V. I., Jr. *Struct. Chem.* **1982**, *23*, 62.
(25) Ermakov, A. A. Kirichenko, E. I.; Pimkin, N. I.; Chizhov, Y. V.; Kleimenov, V. I. *J. Struct. Chem.* **1982**, *23*, 539.

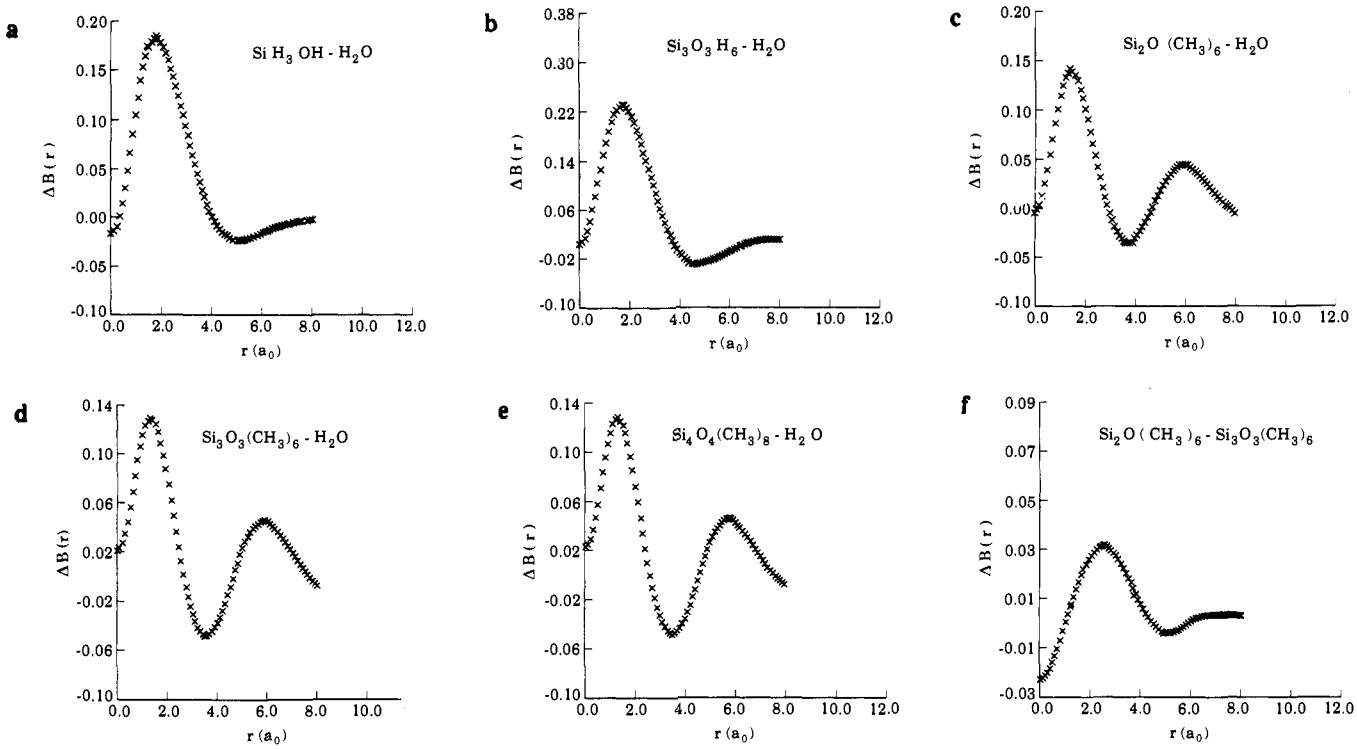

Figure 6. Calculated $\Delta B(r)$ for various orbital pairs.

successively substituted for H is similar to effects seen for the N p "lone-pair" in the $(CH_3)_aH_bN$ series. CH_3H_2N shows only a single peak around 1.0 au, but additional peaks (at the origin for this a_1 symmetry orbital) occur for $(CH_3)_2HN$ and $(CH_3)_3N$.[26]

To obtain a position space interpretation of the orbital $\rho(q)$, we have Fourier transformed them to produce one-dimensional $B(r)$ functions and have then taken $B(r)$ function differences with respect to H_2O. The calculated $\Delta B(r)$ functions are given in Figure 6. As we have shown,[7] $\Delta B(r)$ can be approximated as $\Delta B(r) = \int \bar{\psi}_{ij}(s)\Delta\psi_{ij}(s + r)\, ds$ where $\bar{\psi}_{ij}(r) = {}^1/_2(\psi_i(r) + \psi_j(r))$ and $\Delta\psi_{ij}(r) = \psi_i(r) - \psi_j(r)$.

A graphical representation of this approximation can be used to explain the form of $\Delta B(r)$ as illustrated by the pictograms in Figure 5 for the simple case of the σ_g and σ_u orbitals of a homonuclear diatomic. Pictograms of $\psi_{\sigma g}(r)$ and $\psi_{\sigma u}(r)$ are given in Figure 5a,b, the corresponding momentum distributions in Figure 5c, the $\Delta B(r)$ function in Figure 5d, and the one-electron wave function average and difference, $\bar{\psi}(r)$ and $\Delta\psi(r)$, in Figure 5e,f. One can show algebraically that for this simple case $\Delta B(r)$ has a minimum at a distance equal to the internuclear distance, R. Equivalently, the minimum in $\Delta B(r)$ may be associated with the presence of oppositely signed extrema in $\bar{\psi}(r)$ and $\Delta\psi(r)$ which are separated by R. If $\bar{\psi}(r)$ is known reasonably well, we obtain direct information on $\Delta\psi(r)$, the change in wave function from one case to another, by analyzing $\Delta B(r)$. Such an analysis may of course be hindered by the absence of directional information in $\Delta B(r)$ for unsymmetrical molecules and delocalized orbitals. For interactions between relatively diffuse orbitals on nearest neighbor atoms, e.g. C 2pπ orbitals in conjugated hydrocarbons, extrema in $\Delta B(r)$ occur at distances somewhat shorter than the bond distance.[27]

All the calculated $\Delta B(r)$ plots for the cyclic –H compounds show maxima at about 1.6 a_0 and minima around 4.7 a_0. For the methylated species these features are shifted to somewhat smaller distances, about 1.3 and 3.5 a_0, and another maximum arises at 5.8 a_0. These $\Delta B(r)$ plots can be understood semiquantitatively by inspection of position space plots of the HOMO's in Figure 7. The $1b_1$ HOMO of water is essentially an O 2pπ orbital while the $Si_3O_3(CH_3)_6$ HOMO has predominant O 2pπ character but also has secondary contributions from a p orbital on the Si having the same sign as the O 2p and a p orbital centered on C of opposite sign to the O 2p. For the –H compounds (such as $Si_3O_3H_6$) plots of the HOMO's show predominant O 2pπ character with small bonding contributions from the Si p orbitals and large antibonding contributions from the H s orbitals. Our calculated HOMO electron distributions for the –H compounds are at least qualitatively the same as those found for the HOMO of $Si_2O_2H_4$ by Bachrach and Streitweiser.[28] The $\Delta B(r)$ maximum in these siloxanes at around 1.6 a_0 (compared to an Si–O distance around 3.1 a_0) can be attributed to the bonding interaction of the O 2pπ with a p orbital lobe on Si. The minimum around 4.7 a_0 in the –H compounds can be attributed to the antibonding interaction of the O 2pπ with a H 1s orbital (the O–H distance is 4.8 a_0). In the methylated compounds the minima at about 3.5 a_0 and the maxima at about 5.8 a_0 arise from the two lobes of the C p orbital seen in Figure 7 (the O–C distance is 5.4 a_0). Thus the $\Delta B(r)$ and the $\rho(q)$ plots are different in the –H compared to the $-CH_3$ compounds because of the different compositions of the Si–R σ^* orbital component interacting with the O 2pπ.

A comparison of $Si_2O(CH_3)_6$ and $Si_3O_3(CH_3)_6$ using calculated $\rho(q)$ and the $\Delta B(r)$ approach is also shown in Figure 6. The feature around 2 a_0 arises from differences in the nature of the O–Si bonding while the minimum at about 4.9 a_0 can be attributed to the bonding interaction between O atoms in the ring species, since the O–O separation is 4.94 a_0. Note however that the $\Delta B(r)$ extrema are very small for the $Si_2O(CH_3)_6$–$Si_3O_3(CH_3)_6$ pair, due to the essential similarity of their $\rho(q)$ distributions.

Directly comparing experimental and calculated $\Delta B(r)$ functions is difficult due to systematic and random errors in the experimental data, particularly in the high-momentum region, as well as approximations in the calculations. Distorted wave effects cause the experimental cross section to be systematically higher than that calculated within the plane wave impulse approximation for

(26) Bawagan, A. O.; Brion, C. E. *Chem. Phys.* **1988**, *123*, 51.
(27) Moore, J. H.; Tossell, J. A.; Coplan, M. A. *Acc. Chem. Res.* **1982**, *15*, 192.
(28) Bachrach, S. M.; Streitweiser, A. *J. Am. Chem. Soc.* **1985**, *107*, 1186.
(29) Fink, M. J.; Haller, K. J.; West, R.; Michl, J. *J. Am. Chem. Soc.* **1984**, *106*, 822.
(30) Glidewell, C.; Robiette, A. G.; Sheldrick, G. M. *J. Chem. Soc., Chem. Commun.* **1970**, 931.

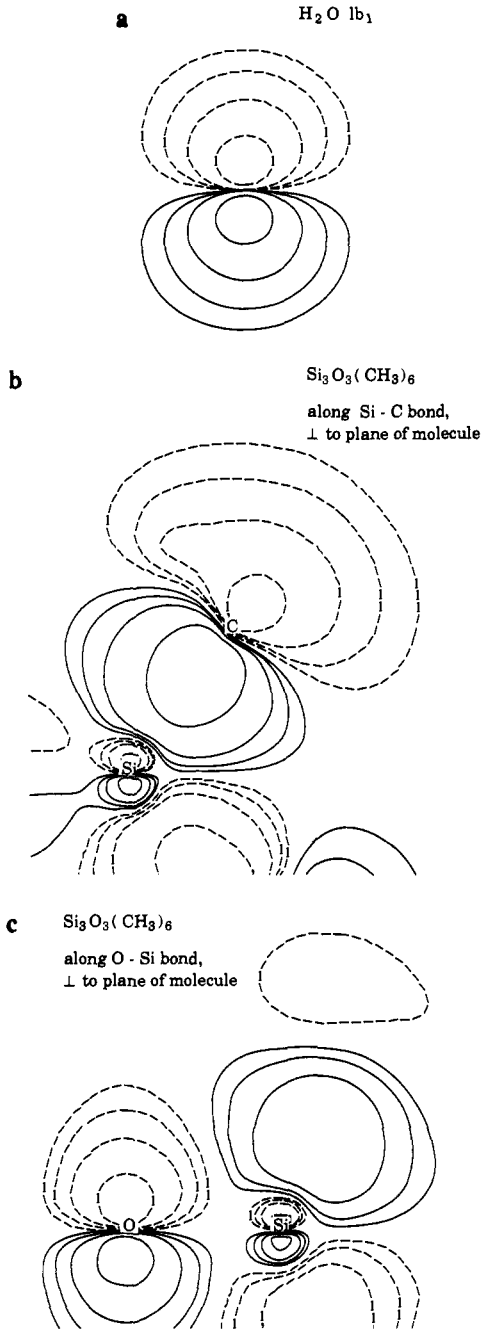

Figure 7. Calculated $\psi(r)$ for HOMO's of H_2O and $Si_3O_3(CH_3)_6$ in indicated planes.

$q \geq 2.4$ au. The percent random error in the data is also considerably higher for $q > 1.6$ au. Since the $\rho(q)$ contribution to $B(r)$ is weighed by the integrating factor q^2, this causes a considerable error in $\Delta B(r)$. In our particular experimental arrangement there are also very few data points between 1.9 and 2.4 au, so the shape of the $\rho(q)$ plot is not well constrained in this region. In the Fourier transformation of our experimental $\rho(q)$ data we therefore integrate only from 0–2.0 au. A similar truncation of the q range was used in calculating theoretical $\Delta B(r)$'s between the siloxanes and H_2O and the resultant theoretical values of $B(0)$ (equal to 1.0 when integrated over all space) were used to normalize the experimental $B(r)$'s. For an integration range of 0–2.0 au the calculated $B(0)$ values were around 0.85. That is, only about 15% of the electron density lies beyond a momentum of 2.0 au. To make our comparison of the siloxanes and water as accurate as possible we have also required a new $\rho(q)$ distribution for the $1b_1$ HOMO of H_2O at the same energy and momentum resolution as for the siloxanes.

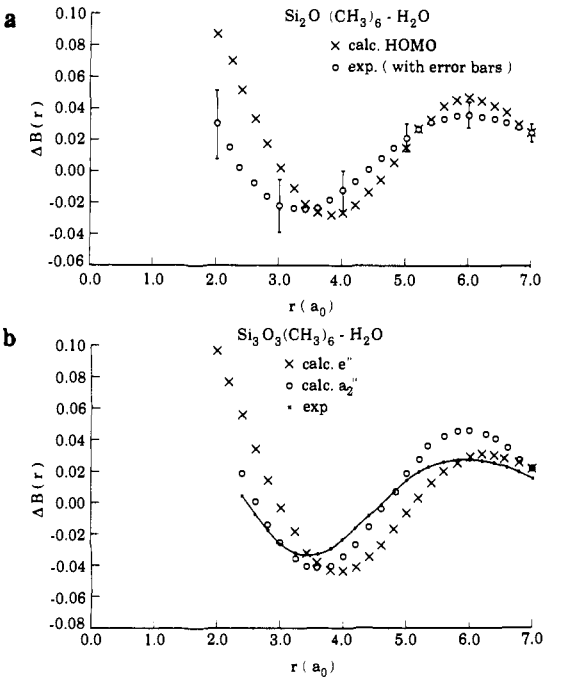

Figure 8. Comparison of experimental and calculated truncated $\Delta B(r)$ for indicated orbital pairs (integration range is 0–2.0 au of momentum).

Truncation of the integration at 2.0 au of momentum unfortunately wipes out the $\Delta B(r)$ maxima around 1.5 a_0 associated with Si p orbital participation seen in Figure 6—$\Delta B(r)$ for the siloxanes vs H_2O simply continues to increase approaching $r = 0$. Fortunately the extrema associated with the C 2p orbital contributions between about 3 and 7 a_0 remain, only slightly shifted in position and magnitude by the truncation. The calculated and experimental $\Delta B(r)$ functions comparing the HOMO's of $Si_2O(CH_3)_6$ and $Si_3O_3(CH_3)_6$ and the H_2O $1b_1$ MO are shown in Figure 8.

We have calculated the random errors in our experimental $B(r)$ and $\Delta B(r)$ functions assuming a Gaussian distribution of random error in $\rho(q)$. Calculated error bars are shown on the experimental $\Delta B(r)$ plot for $Si_2O(CH_3)_6$ vs H_2O at 1 a_0 intervals (Figure 8). It is clear that in the region $r = 3$–7 a_0 the calculated and experimental $\Delta B(r)$ functions are almost equivalent within experimental error. Calculation and experiment also agree well for the $Si_3O_3(CH_3)_6$–H_2O pair. This direct comparison of (truncated) theoretical and experimental $\Delta B(r)$ functions supports our conclusion that the HOMO's of these siloxanes show C 2p orbital contributions corresponding to an antibonding interaction of the O $2p\pi$ with a C 2p orbital. We have also calculated the $\Delta B(r)$ function for the $Si_2O(CH_3)_6$–$Si_3O_3(CH_3)_6$ pair and we find a minimum around 5.0 a_0 which could be attributed to the O–O interaction in the "3-ring" compound, as seen in the calculated $\Delta B(r)$ plot in Figure 6. Unfortunately, the magnitudes of the extrema in the experimental $\Delta B(r)$ plot for this case are very small (on the order of 0.004), much smaller than our error bars, so that we cannot be sure of their significance.

Conclusion

Momentum distributions for the predominantly O $2p\pi$ highest energy occupied molecular orbitals of both linear and cyclic siloxanes show multiple peak structures in $\rho(q)$ arising from Si 3p and H 1s or C 2p orbital admixture. The interaction is most simply described as the admixture of Si 3p and H 1s or C 2p orbitals with the O $2p\pi$. Although such interactions occur in SiH_3OH as well as in the species where O is bonded to two Si's, their strength is apparently insufficient in SiH_3OH to generate a two-peak structure in $\rho(q)$. The difference in $\rho(q)$ between linear disiloxane and the 3-ring and 4-ring compounds can be attributed partly to the delocalization of the HOMO over the n oxygens in the ring species.

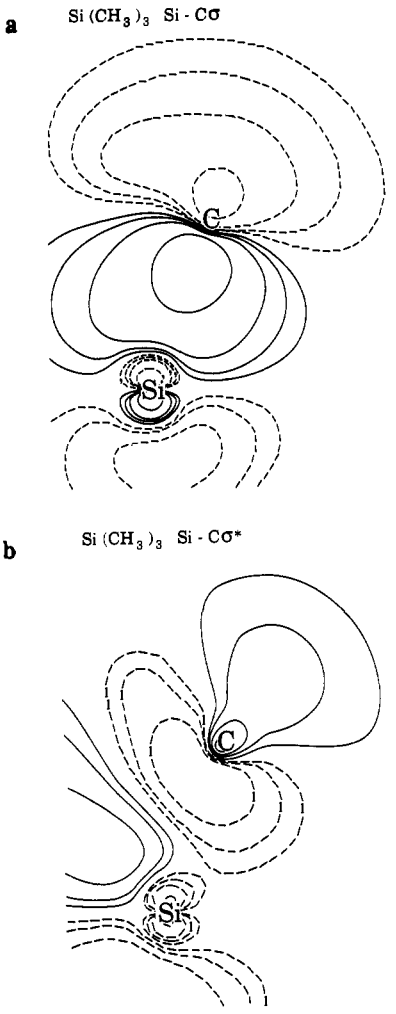

Figure 9. Calculated $\psi(r)$ for HOMO (Si–C σ) and LUMO (Si–C σ^*) in $Si(CH_3)_3$ obtained from an unrestricted Hartree–Fock calculation using the same geometry and basis set as for $Si_3O_3(CH_3)_6$.

The idea of interaction between $p\pi$ orbitals on electronegative atoms like O and σ^* orbitals localized between atoms in α and β positions with respect to them, what might be called $p\pi-\sigma^*$ hyperconjugation, was first developed by Pitt[31] as an alternative to the $p\pi-d\pi$ bonding model. Experimental studies of the energetics of unoccupied orbitals of Si containing molecules using eletron transmission spectroscopy[32] were also more in agreement with a Si–R σ^* model than with a Si 3d model. Recently interpretations of structural properties based on such O $2p\pi$–SiR σ^* bonding model have been used in qualitative MO treatments.[33] Such hyperconjugative interactions have been used to explain Al–O distances in aluminum aryloxides,[34] P–A distances in $M-PA_3$ units,[35] and structures and photoelectron spectra of $SiHR_3$ complexes of metals.[36] However, all these previous studies of $p\pi-\sigma^*$ interaction have been indirect, focusing upon the supposed structural or energetic consequences of such interactions. In the $\Delta B(r)$ plots of Figure 8 we, in effect, "see" directly the C 2p orbital contributions to the siloxane HOMO's.

Although our results unambiguously show substantial C 2p contributions to the siloxane HOMO's, the small Si 3p contribution seems inconsistent with a description of the Si–C interaction as σ antibonding. Shambayati et al.[37] have recently noted that the HOMO electron distribution of Si_2OH_6 can be interpreted in fragment orbital terms as a combination of a nonbonding O $2p\pi$ orbital with an antibonding contribution from a Si–H σ bonding orbital plus a bonding contribution from the Si–H σ^* orbital (i.e., the orbital is $n-\pi(SiH_3) + \pi^*(SiH_3)$ in their notation, see their page 701). Such a combination of destabilizing Si–H σ and stabilizing Si–H σ^* contributions would be expected on the basis of simple qualitative MO arguments and would tend to cancel out the Si 3p character and increase the H 1s character in the HOMO of Si_2OH_6. A previous analysis of destabilizing and stabilizing contributions to the HOMO of Si_2OH_6 based upon orbital ionization potentials by Beach and Jolly[38] led to a similar conclusion, a rather close balance of the energetic effects of destabilizing contributions from interaction with occupied SiH_3 orbitals and stabilizing contributions from interaction with empty SiH_3 orbitals.

To further test these concepts we have calculated $\psi(r)$ plots for occupied Si–C σ and empty Si–C σ^* orbitals of the $Si(CH_3)_3$ radical, using the unrestricted Hartree–Fock method and the same Si–C geometry and basis set as for $Si_3O_3(CH_3)_6$. These two orbital plots are displayed in Figure 9. The first point to note is that the $\psi(r)$ plots for the HOMO of $Si(CH)_3$ (designated in Figure 9 as Si–C σ) and the LUMO (designated Si–C σ^*), which bracket the singly occupied MO (a σ orbital directed along the C_3 axis), both show predominant C 2p character with relatively little Si 3p character. Thus interaction of either one with the O $2p\pi$ of $Si_3O_3(CH_3)_6$ would produce a $\psi(r)$ plot qualitatively like that shown in Figure 7. More quantitatively, the Si–C portion of the $\psi(r)$ plot for the $Si_3O_3(CH_3)_6$ HOMO in Figure 7 looks more like that for the $Si(CH)_3$ Si–C σ HOMO than it does the Si–C σ^* LUMO. Although this is consistent with the arguments presented in refs 37 and 38 the use of a virtual MO to generate $\psi(r)$ for a Si–C σ^* orbital may reduce the meaningfulness of the σ vs σ^* comparison. The most important point is that both the HOMO and LUMO of $Si(CH_3)_3$ are predominantly C 2p in character and that this character shows up in the HOMO's of the methylated siloxanes.

It would be interesting to acquire data for $N(SiH_3)_3$ or its methylated analogue, for which the energy analysis of Beach and Jolly indicates an overall stabilization of the predominantly N 2p "lone-pair" HOMO. Preliminary RHF calculations on $N(SiH_3)$ at the 3-21G* basis level yield an essentially planar geometry ($\angle N-Si-N = 119.8°$), a two-peak $\rho(q)$ for the HOMO, and a $\Delta B(r)$ function between $N(SiH_3)_3$ and NH_3 with a shape much like that for $Si_3O_3H_6$ vs H_2O, indicative of an antibonding interaction between the N 2p and the H 1s orbitals on the $-SiH_3$ group.

To further determine the relationship between the orbital momentum distributions described here and the reactivity of the siloxanes a number of questions must be addressed. First, we should consider whether the interaction of the siloxane O with H^+ or H_2O is indeed mainly through the O $2p\pi$ HOMO's. Calculations on protonated $Si_3O_3H_6$ (in C_s symmetry at the 3-21G RHF level) give a minimum energy for an angle between the direction perpendicular to the Si_3O_6 ring and the O–H bond vector of 64°. According to the argument presented on pages 105–107 of ref 33 this indicates a larger interaction with the O $2p\sigma$ than with the O $2p\pi$ orbitals. A large number of MO's have significant contributions from O 2p orbitals in the plane and directed away from the center of the ring (the analogue of the $3a_1$ MO of H_2O). These orbitals have considerably more negative eigenvalues than the HOMO and are expected to occur in rather broad featureless regions of the siloxane PES. Obtaining experimental momentum distributions for them will be difficult.

Our results indicate that discrimination between "3-ring" and "4-ring" cyclosiloxanes with use of (e,2e) spectroscopy is also very

(31) Pitt, C. G. *J. Organomet. Chem.* **1973**, *61*, 49.
(32) Tossell, J. A.; Moore, J. H.; Giordan, J. C. *Inorg. Chem.* **1985**, *24*, 1100.
(33) Albright, T. A.; Burdett, J. K.; Whango, M. H. *Orbital Interactions In Chemistry*; Wiley: New York, 1985.
(34) Healy, M. D.; Ziller, J. W.; Barron, A. R. *J. Am. Chem. Soc.* **1990**, *112*, 2949.
(35) Orpen, A. G.; Connelly, N. G. *Organometallics* **1990**, *9*, 1206.
(36) Lichtenberger, D. L.; Kellog, G. E. *J. Am. Chem. Soc.* **1986**, *108*, 2560.
(37) Shambayati, S.; Blake, J. F.; Wierschke, S.; Jorgensen, W. L.; Schreiber, S. *J. Am. Chem. Soc.* **1990**, *112*, 697.
(38) Beach, D. B.; Jolly, W. L. *Inorg. Chem.* **1984**, *23*, 4774.

difficult. By contrast it should be easily possible to qualitatively distinguish between "lone-pair" type orbitals on O bonded to one Si and one H and those with O bonded to two Si, simply by inspecting the number of peaks in $\rho(q)$. Extended to solid surfaces this would provide a direct means of monitoring silanol, Si–O–H, and bridging oxygen, Si–O–Si, sites on the surface of a silica glass or silicate mineral.

Acknowledgment. The work was supported by the National Science Foundation, Grants CHE-88-08589 and EAR-86-03499.

Communications to the Editor

Semisynthesis of Axial-Ligand (Position 80) Mutants of Cytochrome *c*

Adrienne L. Raphael and Harry B. Gray*

Contribution No. 8186, Arthur Amos Noyes Laboratory
California Institute of Technology
Pasadena, California 91125

Received August 6, 1990

Axial ligands play important roles in the functions of heme proteins.[1-3] Although changes in axial ligation in cytochrome *c* can be made both by biological and chemical techniques,[4-10] we have found that chemical semisynthesis[7,11] is particularly useful in that it allows the production of reasonable quantities of mutants that vary widely in the electronic character of the axial group at position 80. Of special interest is our finding that substitution of methionine by cysteine (cyt *c*-Cys80)[12,13] results in a mutant protein with a reduction potential of −390 mV, thereby demonstrating that axial ligand replacement alone can shift the reduction potential well over 600 mV from native cytochrome *c* (262 mV).[14]

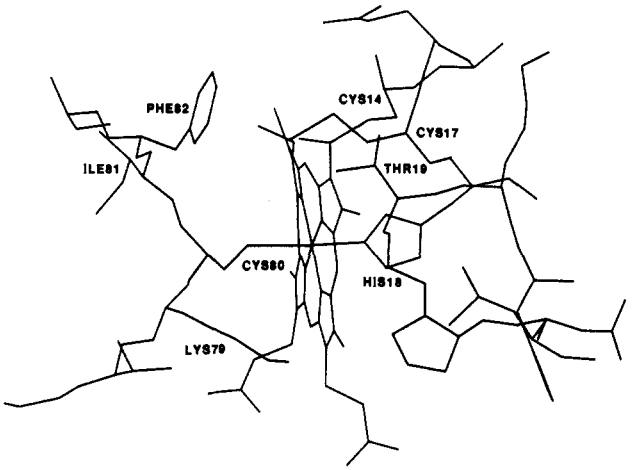

Figure 1. Heme area of cyt *c*-Cys80.

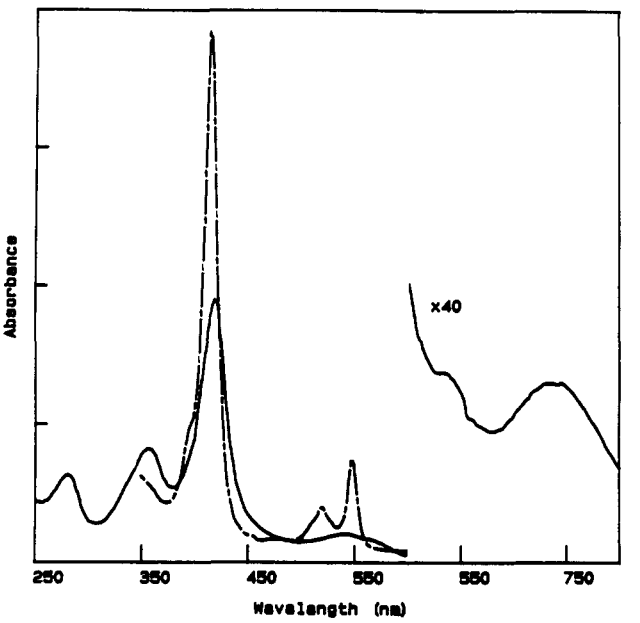

Figure 2. Absorption spectra of oxidized (—) and reduced (- - -) cyt *c*-Cys80 in 50 mM sodium phosphate buffer, pH 7.0.

Ferric cyt *c*-Cys80 also is strikingly similar spectroscopically to cytochrome P-450.

The heme area of cyt *c*-Cys80 is pictured in Figure 1.[15] Proteins with histidine (cyt *c*-His80)[7] and leucine (cyt *c*-Leu80)[16]

(1) Dickerson, R. E.; Timkovich, R. In *The Enzymes*, 3rd Ed.; Boyer, P., Ed.; Academic Press, Inc.: New York, 1975; Vol. 11, pp 397-547.
(2) Wüthrich, K. *Q. Rev. Biophys.* **1985**, *18*, 111-134.
(3) Marchon, J.-C.; Mashiko, T.; Reed, C. A. In *Electron Transport and Oxygen Utilization*, Ho, C., Ed.; Elsevier: North Holland, NY, 1982; pp 67-73.
(4) Hampsey, D. M.; Das, G.; Sherman, F. *J. Biol. Chem.* **1986**, *261*, 3259-3271.
(5) Sligar, S. G.; Egeberg, K. D.; Sage, J. T.; Morikis, D.; Champion, P. M. *J. Am. Chem. Soc.* **1987**, *109*, 7896-7897.
(6) Sorrell, T. N.; Martin, P. K.; Bowden, E. F. *J. Am. Chem. Soc.* **1989**, *111*, 766-767.
(7) Raphael, A. L.; Gray, H. B. *Proteins: Struct., Funct., Genet.* **1989**, *6*, 338-340.
(8) Harbury, H. A.; Cronin, J. R.; Fanger, M. W.; Hettinger, T. P.; Murphy, A. J.; Myer, Y. P.; Vinogradov, S. N. *Proc. Natl. Acad. Sci. U.S.A.* **1965**, *54*, 1658-1664.
(9) Wasserman, G. F.; Nix, P. T.; Koul, A. K.; Warme, P. K. *Biochim. Biophys. Acta* **1980**, *623*, 457-460.
(10) Santucci, R.; Brunori, M.; Ascoli, F. *Biochim. Biophys. Acta* **1987**, *914*, 185-189.
(11) (a) Corradin, G.; Harbury, H. A. *Proc. Natl. Acad. Sci. U.S.A.* **1971**, *68*, 3036-3039. (b) Wallace, C. J. A.; Mascagni, P.; Chait, B. T.; Collawn, J. F.; Paterson, Y.; Proudfoot, A. E. I.; Kent, S. B. H. *J. Biol. Chem.*, submitted for publication. (c) Chaiken, I. M. *CRC Crit. Rev. Biochem.* **1981**, 255-301. (d) ten Kortenaar, P. B. W.; Adams, P. H. J. M.; Tesser, G. I. *Proc. Natl. Acad. Sci. U.S.A.* **1985**, *82*, 8279-8283.
(12) Syntheses involved reaction of 1-65 lactone (CNBr cleavage product of cytochrome c^2) and peptide 66-104.[7,13] Cyt *c*-Cys80 was synthesized by using 0.35 mM 1-65 lactone and peptide 66-104(Cys80) in 5 mM sodium phosphate buffer, pH 7.0, which was degassed and reduced with 4 equiv of sodium dithionite. After reaction under Ar for 36 h at ambient temperature with addition of 0.5 equiv of dithionite every 12 h, the products were purified by using cation-exchange chromatography (Pharmacia FPLC 10/10 Mono S column) with a 0.15-0.40 M NaCl gradient in 0.05 M sodium phosphate buffer, pH 7.0. Isoelectric focusing showed that cyt *c*-Cys80 was one species, with an isoelectric point equal to that of cytochrome *c*. Amino acid analyses agreed well with calculated values (in most cases within 2%).
(13) Peptides 66-104 were synthesized by using a stepwise solid-phase method performed on an ABI 43A synthesizer. Kent, S. B. H. *Annu. Rev. Biochem.* **1988**, *57*, 957-985. Kent, S. B. H.; Parker, K. F.; Schiller, D. L.; Woo, D. D.-L.; Clark-Lewis, I.; Chait, B. T. In *Peptides: Chemistry and Biology, Proceedings of the Tenth American Peptide Symposium*; Marshall, G. R., Ed.; ESCOM: Leiden, 1988; pp 173-178.
(14) Taniguchi, V. T.; Ellis, W. R., Jr.; Cammarata, V.; Webb, J.; Anson, F. C.; Gray, H. B. *Adv. Chem. Ser.* **1982**, *201*, 51-68.
(15) Computer representation of the replacement of Met80 with cysteine and local energy minimization were carried out on the tuna cytochrome *c* structure, modified to the horse sequence (Takano, T.; Dickerson, R. E. *J. Mol. Biol.* **1981**, *153*, 79-94) by using BIOGRAF/III (Biodesign, Inc.).

0002-7863/91/1513-1038$02.50/0